NASA Contractor Report 182191

The Relationship Between Observed Fatigue Damage and Life Estimation Models

Peter Kurath and Darrell F. Socie
University of Illinois at Urbana-Champaign
Urbana, Illinois

August 1988

Prepared for
Lewis Research Center
Under Grant NAG3–465

National Aeronautics and
Space Administration

THE RELATIONSHIP BETWEEN OBSERVED FATIGUE DAMAGE AND LIFE ESTIMATION MODELS

Peter Kurath and Darrell F. Socie
Department of Mechanical and Industrial Engineering
University of Illinois at Urbana-Champaign
Urbana, IL 61801

SUMMARY

Observations of the surface of laboratory specimens subjected to axial and torsional fatigue loadings has resulted in the identification of three fatigue damage phenomena; crack nucleation, shear crack growth, and tensile crack growth. Material, microstructure, state of stress/strain, and loading amplitude all influence which of the three types of fatigue damage occurs during a dominant fatigue life fraction. Fatigue damage maps are employed as to summarize the experimental observations. Appropriate bulk stress/strain damage parameters are suggested to model fatigue damage for the dominant fatigue life fraction. Extension of the damage map concept to more complex loadings is presented.

NOMENCLATURE

b, b_o	Axial, torsional fatigue strength exponent
c, c_o	Axial, torsional fatigue ductility exponent
E, G	Axial, shear linear elastic modulus
k	Biaxial material constant
N_f	Cycles to failure
$2N$	Reversals
$\Delta\gamma/2$	Shear strain amplitude
$\Delta\varepsilon_n/2$	Strain amplitude normal to a shear strain direction
$\Delta\varepsilon_1/2$	Principal strain amplitude
$\Delta\tau/2$	Shear stress amplitude
$\Delta\sigma_1/2$	Principal stress amplitude
$\varepsilon_f', \gamma_f'$	Uniaxial, torsional fatigue ductility coefficient
σ_f', τ_f'	Uniaxial, torsional fatigue strength coefficient
σ_{no}	Mean stress normal to a shear strain direction
σ_y	Yield stress
σ_n^{max}	Maximum stress normal to a shear strain direction
σ^{max}	Maximum stress in the direction of the principal strain

1. INTRODUCTION

Fatigue life estimates represent one aspect of durability assessment of components and structures. Bulk deformation models for fatigue life prediction analyses include both stress-life and strain-life approaches, the latter being more appropriate for deformations involving plastic strains. These approaches are most often employed to assess the influence of changes in service usage, material or local geometry on the fatigue life. The resulting life estimate may include a substantial fatigue life fraction of micro crack growth relative to the total fatigue life which is not adequately described by traditional fracture mechanics approaches, as well as some long crack growth. Often microcrack formation and growth consume the majority of the usable fatigue life in a component or test specimen. Although both crack formation and growth are recognized as contributing factors to the fatigue life, bulk deformation data are often interpreted as the life to some arbitrary crack size, and are often referred to as crack initiation approaches.

In bulk deformation models, stresses and strains in the critical location (usually a geometric feature) are assumed to govern the fatigue life. Cracks are assumed to nucleate and grow in the structure in the same manner as in the smooth laboratory specimens that are used to determine the baseline fatigue properties. Even for the materials category of metals, no universally acceptable fatigue damage model has been forwarded. Numerous fatigue damage models have been formulated to relate simple laboratory tests to more complex stress states [1,2]. Almost any of these models provides reasonable correlation for one simple laboratory stress or strain state. For extrapolation of damage models to other stress-strain states recognition of the physical damage process is required to select the most appropriate fatigue

damage model. Material (including processing variables), stress or strain amplitude, and state of stress are some of the factors which should influence this choice.

1.1 Background

August Wöhler, while not the first, is one of the more famous early fatigue researchers. During the period from about 1850 to 1875, experiments were conducted to establish a safe alternating stress below which failure would not occur [3]. Full scale axles as well as smaller laboratory specimens were employed to establish the endurance limit concept for design. It should be noted that the laboratory rotating bending test which Wöhler developed in many respects mirrors the component loading. Nearly one hundred years of research has been performed to experimentally establish the effects of the many variables that influence the long life fatigue strength of metals.

In 1903 Ewing and Humphrey [4], motivated by the work of Wöhler and Bauschinger, published their classic paper. Flat fatigue specimens made from high quality Swedish iron were tested in the annealed condition. Optical microscopy was employed to examine the same region of the specimen at various stages during the fatigue life. They stated, "The coarse of the breakdown was as follows: --The first examination, made after a few reversals of the stress, showed slip-lines on some of the crystals, ... the slip-lines were quite similar in appearance to those which are seen when a simple tensile stress exceeding the elastic limit is applied ... After many reversals they changed into comparatively wide bands with rather hazily defined edges, ... As the number of reversals increased this process of broadening continued, and some parts of the surface became almost covered with dark markings ... When this stage was reached it was found that some of the crystals had cracked. The

cracks occurred along broadened slipbands; in some instances they were first seen on a single crystal, but soon they joined up from crystal to crystal, until finally a long continuous crack was developed across the surface of the specimen." Slip bands observed were oriented in the direction of maximum shear stress. In addition, the authors recognized that: "Once an incipient crack begins to form across a certain set of crystals, the effect of further reversals is mainly confined to the neighborhood of the crack." Thus, at the turn of the century, an understanding of the basic cause of fatigue for many wrought metals, to-and-fro slip, was established. Later work using electron microscopy, X-ray techniques and other powerful tools has provided further substantiation that the basic cause of fatigue crack nucleation in many metals is a result of alternating shear stresses and strains.

Forsyth [5] noted that slip band cracking is dependent on the shear stress range acting on the slip plane. Therefore, it was hypothesized that cracks would initiate in the maximum shear stress orientation, which is referred to as Stage I cracking direction. Fatigue crack propagation can occur on the same plane as crack initiation or it can occur on planes perpendicular to the maximum principal stress. Forsyth referred to propagation perpendicular to the maximum principal stress as Stage II cracking. This change in cracking direction is dependent upon strain amplitude, loading mode, state of stress, and material type.

State of stress effects were studied by several investigators with the work of Gough [6] being noteworthy. Studies of the fatigue limit in bending and torsion were performed and results indicated that the ratio of the fatigue limit in torsion to that in bending varied with material tested. These observations lead to models that would reduce to the maximum shear stress theory for ductile materials and the maximum principal stress theory for

brittle materials such as mild steel and cast iron, respectively. Guest [7] also proposed a single model with a material dependent constant that could change the theory from maximum shear stress to maximum principal stress. These formulations were among the first to incorporate the failure mode of the material in the damage model.

This early research showed that it is not necessary to consider the entire fatigue process in order to make engineering estimates of the fatigue life of a structure or component. Rather, a model that is representative of the damage process during the majority of the fatigue life is sufficient. The ensuing discussion will focus on the implementation of bulk deformation models for biaxial stress-strain states. Fatigue damage observations for two materials will be employed to justify the life analysis methods proposed.

2. FATIGUE DAMAGE

2.1 Damage Maps

Observation of the surface of a laboratory specimen subjected to cyclic loading has been employed by many researchers [4,5,8-13] to characterize fatigue damage. For metals, three regimes of fatigue damage have been noted: 1) crack formation, 2) crack growth oriented with the maximum shear stress or strain amplitude, and 3) crack growth perpendicular to the maximum principal stress or strain amplitude. Material, loading amplitude, and stress-strain state will influence the type of fatigue damage occurring. Different bulk deformation stresses and/or strains may adequately characterize each of the three types of fatigue damage observed. The dominance of one of these phenomena should dictate the choice of bulk deformation parameters chosen for the damage parameter.

For a given material and stress-strain state a damage map (Fig. 1) is employed to illustrate the change in fatigue damage with fatigue life (i.e. change in stress or strain amplitude). The vertical axis for this plot is in terms of fatigue life fraction and the horizontal scale represents total fatigue life. An arbitrarily chosen surface crack dimension is employed as a demarcation between crack formation and growth, and is represented by the solid line. It could be argued that nucleation occurs at some other observable dimension, but this would simply shift the line without changing the qualitative phenomena represented by the plots. The dashed line separates observed crack growth perpendicular to the maximum principal stress or strain amplitude direction from crack growth along a shear direction. If any one damage model were appropriate for the entire range of fatigue life, then the solid and dashed lines would be horizontal. Horizontal lines in Figure 1 would imply that regardless of fatigue life, identical life fractions of crack

nucleation, shear crack growth and tensile crack growth would be observed in a material. The fatigue analysis would then reflect the dominant damage mechanism. Three regions of fatigue damage are noted in these plots. In Region A shear crack growth dominates the fatigue life fraction. Region B is characterized by crack nucleation and perhaps some Stage I crack growth followed by a dominant life fraction of crack growth perpendicular to the maximum principal strain amplitude (Forsyth's Stage II cracking). Crack nucleation is the dominant life fraction in Region C. Damage maps are employed in the ensuing discussion to formulate appropriate damage models for specific materials.

Detailed crack observations have been made on two materials, AISI 304 stainless steel and Inconel 718. These materials exhibit different regions of fatigue damage, and illustrate discrepancies with regard to the type of damage classically assumed for ductile and brittle materials. Experimental data and crack observations can be found in earlier publications [12,14]. Two regions, Regions A and B, are shown in Fig. 2 for AISI 304 stainless steel tubular specimens loaded in torsion. A crack dimension of 0.1 mm was used as a demarcation between crack nucleation and crack growth for this material (i.e. solid line). In Region A, microscopic observations of specimen surface acetate tape replicas showed that cracks initiated in the maximum shear strain amplitude orientation and at grain boundaries. Once initiated, the cracks became more distinct but showed no significant increase in length. At failure, a large density of small, coarse cracks dominated the surface of the specimen. A small amount of branching onto tensile planes (Stage II planes) was observed late in the fatigue life. Macroscopic failure cracks grew in either a shear orientation (Stage I) or tensile (Stage II) direction by linking of previously initiated shear cracks. Region B behavior was observed

at intermediate fatigue lives in torsion (5×10^4 to 2×10^6 cycles). The fraction of fatigue life spent growing the crack in a shear direction was reduced, as was the crack density for this range of fatigue lives. A small number of shear cracks initiated but quickly branched to a Stage II direction. Growth of these cracks occurred by the propagation of the main crack rather than by a linking process. Although no region C behavior was experimentally observed for torsional loading, the data trends would infer its existence at fatigue lives greater than 10^7 cycles.

Surface replicas and scanning electron microscopic examination of the fracture surfaces of AISI 304 specimens tested in tension revealed no perceptible shear crack growth. As a result, no Region A behavior is shown in Fig. 3. It should be noted that uniaxial solid specimens with a 6 mm gage diameter were used for the tension experiments with 304 stainless steel while tubular specimens were employed for all the loading cases discussed. Fractography revealed that striations could be traced to the origin of the failure crack [15]. Forsyth [9] has categorized striations as either brittle or ductile. Brittle striations are observed to propagate along crystallographic facets (i.e. grain boundaries), whereas ductile ones are essentially parallel to the fracture surface. (It should be noted that ductile striations are those associated with the beach mark pattern typically attributed to striations.) Brittle striations were typical at the point of origin of the failure crack for all except the highest strain amplitude (shortest life tests). Crack formation was the dominant life fraction for all cyclic tensile tests conducted, even though plasticity was observed throughout the fatigue life range (10^2 to 10^6) for all specimens. Hence for axial loading, only Region C is depicted in Fig. 3 for AISI 304. This does not imply that there was no shear or tensile crack growth, merely that crack growth from a 0.1 mm

dimension was not the dominant life fraction. Use of an alternate crack dimension, such as 0.01 mm, would probably result in a Region B for this loading condition.

The torsional behavior of Inconel 718 tubular specimens is summarized in Fig. 4. Again a 0.1 mm crack dimension was used as an experimental demarcation between initiation and propagation phenomena. Unlike the stainless steel which displayed mixed behavior, results of the Inconel 718 torsion tests showed that cracks nucleated and grew in a maximum shear strain amplitude direction. Region A behavior was observed at all values of shear strain amplitude investigated (10^2 to 10^6 cycles). Even at the lowest strain amplitude, for which the nominal stress-strain response was essentially elastic, cracks initiated and remained on shear planes throughout the life. Crack density decreased with increasing fatigue life as it did in 304 stainless steel but no branching onto tensile planes was observed. Again, the life range tested did not reveal either Region B or C behavior, though at longer fatigue ($>10^7$) they may dominate the fatigue process.

Final failure in all tension tests of Inconel 718 was in a macroscopic tensile direction. For short and intermediate fatigue lives a substantial amount of microscopic shear formation and growth was observed, and is reflected by Region A in Fig. 5. Low cycle fatigue damage accumulation in Inconel 718 appears to be shear dominated. The high density of precipitates in this material restricts slip to localized regions. Crack propagation then occurs along the bands with extensive shear crack growth exhibited throughout the fatigue life investigated (10^2 to 10^6 cycles). Stage II crack growth may occur at longer fatigue lives ($>10^7$), but since in this life regime crack nucleation plays the dominant role, it would be classified as Region C. One could argue that using an alternate definition of an initiated crack, there

could conceivably be a Region B for this tensile data. For tensile loading cracks grow in a shear orientation on a scale of 0.1 to 0.2 mm, and perpendicular to the principal strain direction on a scale of 1 mm. Therefore the crack growth for a portion of the fatigue life could be interpreted as either tensile or shear. The absence of Region B will be discussed in a subsequent section.

Ease of experimental testing has resulted in much of the multiaxial research employing combinations of axial and torsional loads (bending-torsional loading is considered to be part of this category). For both materials investigated combined axial-torsional loads resulted in damage maps whose characteristics were bounded by the axial only and torsional only cases. As an initial effort to incorporate state of stress into the damage modeling process, the hydrostatic stress was employed in Figs. 6 and 7 for AISI 304 and Inconel 718 respectively to summarize individual loading conditions. Hydrostatic stress is the vertical axis and fatigue life is the horizontal axis. Torsion, tension and biaxial-tension have normalized hydrostatic stresses of 0, 1/3, and 2/3, respectively. One may choose some deformation parameter such as strain range should be chosen for the horizontal axis rather than fatigue life. Since different bulk stress-strain deformation parameters will best represent the fatigue damage for the three regions proposed, it remains a perplexing problem of which variable to choose. Once a damage parameter has been established to represent a particular region a similar plot could be constructed with a band of validity for that parameter versus some state of stress term such as hydrostatic stress, which for the two materials discussed renders an adequate representation for combined loading cases.

2.2 Fatigue Models

Once the dominant life fraction leading to failure has been identified, an appropriate life estimation model can be selected. Each region may require a separate damage model that is based on the fatigue damage observations. The following damage models are proposed, although it is important to note that alternative methods could have been selected as long as the model captures the driving force for the fatigue damage observed. Bulk stress-strain deformations were chosen to represent the driving force for each fatigue damage region.

2.2.1 Region A

Crack formation and growth in the direction of maximum shear strain amplitude was the dominant damage feature observed for this region, hence maximum shear strain amplitude will be the primary bulk stress-strain parameter chosen to represent fatigue damage. Since this type of fatigue damage is often typical of low cycle fatigue, incorporation of strain rather than stress mirrors other researchers efforts when modeling this life regime. The torsion test has only shear strains and stresses in the maximum shear strain amplitude orientation, and displays a larger Region A than any of the other strain states. Other combinations of tension and torsion may have crack growth in the direction of the maximum shear strain amplitude, however other stresses and strains normal to this plane are present. A classical fracture mechanics approach to this type of cracking would consider a mixed mode stress intensity factor. For a bulk deformation approach, additional terms reflecting the normal stress and/or strains would serve an analogous purpose. This notion has been imbedded in previous high cycle bulk stress life predictive methods for some time. Nadia [16] quoted Mohr: "The shearing stress, S_s, in the

planes of slip reaches, at the limit, a maximum value dependent on the normal stress, S_n, in the same planes." Findley [17] later states, "The principle stress (maximum shear stress) theory modified by the influence of the complementary normal stress may be the most satisfying theory for combined stress fatigue." Similar arguments have been forwarded by Orowan [18] with regard to dislocation motion.

The following model was proposed by Kandil, Brown and Miller [19] and modified by Socie, Kurath, and Koch [14] to include mean stress effects.

$$\frac{\Delta\gamma}{2} + \frac{\Delta\varepsilon_n}{2} + \frac{\sigma_{no}}{E} = \gamma_f' (2N)^{c_o} + \frac{\tau_f'}{G} (2N)^{b_o} \qquad (1)$$

In this approach maximum shear strain amplitude is modified by the strain amplitude and mean stress normal to the maximum shear strain amplitude. These terms are interpreted to account for changes in crack closure that have been observed for different stress-strain states. The right hand side of the equation represents the constants generated from fully reversed torsional testing. Differences in interpretation could arise for out-of-phase loadings, where the maximum value of the composite parameter could differ from the value of the parameter on the maximum shear strain amplitude plane [15]. Constants for the non-shear strain terms have been proposed and may be calculated using fatigue-life results for other stress-strain states [20].

Recently for materials which display Region A, damage and exhibit substantial out-of-phase hardening, an alternate shear based model has been forwarded by Fatemi and Socie [21]. Fatemi and Kurath [22] evaluated the applicability of this parameter for multiaxial mean-stresses loadings.

$$\frac{\Delta\gamma}{2}\left(1 + k\frac{\sigma_n^{max}}{\sigma_y}\right) = \gamma_f' (2N)^{c_o} + \frac{\tau_f'}{G} (2N)^{b_o} \qquad (2)$$

The maximum stress normal to the maximum shear strain amplitude is the modifying parameter employed in this approach. This format also reflects that no shear direction growth should occur in a shear orientation if no shear alternation occurs for a fatigue event. This concept should play a greater role when variable amplitude and out-of-phase biaxial loadings are investigated. The maximum normal stress term allows experimentally observed out-of-phase hardening to be incorporated in the damage parameter, while mean normal stress would not. Again the constant, k, may be calculated by employing fatigue life results for other stress-strain states.

Torsional strain-life constants are employed in these analyses because the torsion test is most likely to display Region A fatigue damage. Only tests displaying Region A behavior should be used when fitting the torsional strain-life constants. It should be noted that both Eqs. (1) and (2) are identical for the torsional test. Also, both equations have been related to uniaxial constants, but since the uniaxial test is less likely to display Region A behavior and the other modifying terms are present for uniaxial testing, the implementation of torsional test data is more appropriate from a conceptual and physical standpoint.

2.2.2 Region B

Crack growth is again a dominant fatigue life fraction for this region as was the case in Region A. However crack growth perpendicular to the maximum principal strain plays a dominant role. The primary bulk deformation for Region B would be maximum principal strain amplitude. This would imply the traditional strain-life approach be invoked. Mean stress has been shown to effect the fatigue life of uniaxial specimens. Smith, Watson, and Topper

[23] proposed a uniaxial parameter to account for mean stress effects which was modified for multiaxial loadings by Bannantine and Socie [12].

$$\frac{\Delta\varepsilon_1}{2}(\sigma^{max}) = \sigma_f'\varepsilon_f'(2N)^{b+c} + \frac{\sigma_f'^2}{E}(2N)^{2b} \qquad (3)$$

In this format the maximum principal strain amplitude is modified by the maximum stress in the direction of maximum principal strain amplitude that occurs during a cycle. For in-phase loadings, where principal stress and strain directions coincide, there is no difference between this interpretation and the maximum value of the composite parameter. Again for out-of-phase loadings discrepancies exist [15]. The maximum value of the composite parameter does not always coincide with the plane of maximum principal stress. As with Eq, (2) the maximum stress term allows experimentally observed or analytically predicted out-of-phase hardening to be incorporated in the damage parameter.

Since Region B fatigue damage is more dominant in the uniaxial test than in torsional testing, axial strain life constants are conceptually appropriate and more practical for this analysis. Again only uniaxial tests which display Region B behavior should be employed to fit the strain life constants.

2.2.3 Region C

Crack formation dominates Region C damage accumulation. The macroscopic crack direction observed for failure renders minimal information for this region since it comprises such a minimal life fraction. In the longer life region, which is typical of Region C, two types of fatigue damage may occur; i) highly localized shear slip and ii) dominance of defects or grain boundaries in fatigue damage accumulation.

Nisitani [24] and Nisitani and Kawano [25] made extensive observations of long life fatigue failures in low carbon steels. They concluded that at the fatigue limit, cracks formed within single grains but were unable to propagate into neighboring grains because of the differences in crystallographic orientation. Hence long life damage could be controlled by cyclic shear stresses. For cases where classical slip concepts of fatigue are appropriate the concepts of Findley [19] are appropriate

$$\frac{\Delta\tau}{2} + \sigma_n = \tau_f'(2N)^{b_o} \qquad (4)$$

For nominally elastic in-phase loadings it should be noted that Eqs. (1) and (4) are identical. Similarities to the terms in Eq. (2) can also be identified. For materials where this extension of these models is appropriate, the fatigue damage at a macroscopic crack tip and for macroscopic cracks are probably identical. It is cautioned, and will be the subject of subsequent discussion that a distinct Region A does not imply that Region C behavior can be modeled with Eq. (4).

It is postulated that other materials are flaw dominated at longer fatigue lives, or microstructurally have a greater ability to resist slip failure, hence a tendency to develop tensile damage, at lower strain or stress amplitudes. Region C behavior for these materials can be modeled using Eq. (3) converted to a stress format;

$$\frac{\Delta\sigma_1^{max}}{2}\,\sigma^{max} = \sigma_f'^{2}\,(2N)^{2b} \qquad (5)$$

It is assumed that the deformation at the critical location is elastic for both Eqs. (4) and (5). If nonlinear behavior (i.e. nominal plasticity) is

present, extensions of Eqs. (1) and (2) or Eq. (3) are suggested for Eqs. (4) and (5), respectively. The common feature of these damage models is that they are evaluated on an orientation consistent with the observed damage phenomenon that dominates the fatigue life fraction. Bulk deformation terms are chosen to reflect the dominant fatigue life fraction damage characteristics.

3. DISCUSSION

Inconel 718 and AISI 304 stainless steel were chosen for discussion because they illustrate agreements and differences commonly associated with ductile and brittle metals. True fracture strains of 0.33 and 1.61 have been reported for monotonic tensile tests of Inconel 718 and AISI 304, respectively. During cyclic loading the stainless steel displayed nominally plastic deformation even at fatigue lives greater than 10^6 cycles, while the nominal deformation was elastic at lives greater than 10^4 cycles for Inconel 718. Classical concepts would dictate that shear type failures are more likely for the more ductile material. Surface crack observations [12,14] refute this concept for the low cycle fatigue of these materials.

For most of the Inconel 718 specimens tested shear crack formation and growth dominated the fatigue damage accumulation. This implies Region A dominance, hence damage modeling via a shear parameter. Fifteen biaxial strain paths including mean-stress and out-of-phase loadings were investigated [14]. When a shear based parameter, Eq. (2), is employed to evaluate the data, it falls within a reasonable scatterband (Fig. 8). Torsional baseline data was used to construct the solid line in Fig. 8. It should be noted that this material experienced little out-of-phase hardening, and that implementation of Eq. (1) for this material provides comparable results. Axial or bending combined with torsional loading comprise the majority of the biaxial data examined. Recent research [26] for biaxial-tension loadings has indicated that shear damage also dominates for this stress state at shorter fatigue lives ($>10^5$ cycles), but that Eq. (2) better represents the experimental fatigue results. It is interpreted that the stress normal to the maximum shear direction rather than the normal strain alters the damage accumulation behavior.

Uniaxial fatigue behavior of Inconel 718 can be fit utilizing the traditional strain-life approach. If the damage mechanism is not properly understood, and Eq. (3) is used to quantify the fatigue data in Fig. 8, the scatter in the data increases considerably (Fig. 9). The solid line in Fig. 9 represents the fully reversed uniaxial baseline data. Most of the uniaxial testing was conducted at strain amplitudes that resulted in fatigue lives less than 10^6 cycles. Since Region A damage is characteristic of these specimens, it is conceptually incorrect to employ these data to fit Eq. (3). This error is reflected in the lack of correlation when considering other stress-strain states. Macroscopic observations of the tensile specimens at failure would reveal an appreciable dimension of Stage II crack growth. However, examination of acetate tape replicas of the specimen surface taken periodically during the fatigue life reveal that small crack growth in a shear orientation dominated the fatigue life fraction. Examination of the fracture surface can provide useful information regarding the mode of failure, however the dimension of Stage I and Stage II crack growth regions are not necessarily indicative of their life fraction. In other words at failure, the lack of a Stage II cracking region can imply that it is not a dominant life fraction. However, its presence does not imply that a dominant life fraction was Stage II cracking or Region B behavior. Periodic observations are required to establish the material's fatigue damage accumulation characteristics.

Inconel 718 is a nickel-based superalloy strengthened by γ' and γ'' superalloy precipitates (precipitate size ~ 300-400 Å), with some carbides at the grain boundaries. The purpose of the precipitates is to impede crystallographic slip due to mechanical loading and resist plastic deformation at higher temperatures. At higher stress levels (i.e. higher strain amplitudes) cracks originate at carbides which serve as stress concentrators [27]. The

precipitates are subsequently sheared at these stress-strain levels, leading to a dominance of shear cracks resulting in failure.

While at longer fatigue lives the carbide particles would continue to serve as initiation sites, the reduced stress level probably is insufficient to shear the precipitates. The carbide particle size and shape could play a dominant role in the number of cycles required to initiate a fatigue crack. When the crack is initiated, it rapidly propagates as a Stage II crack, during a nominal life fraction. This would imply defect dominance of this material at longer fatigue lives similar to that observed for cast iron at short and long fatigue lives. The scatter of the fatigue data increases dramatically at longer fatigue lives for Inconel 718, similar to the observations over the entire life range for defect controlled materials such as cast iron. Hence Eq. (5) is appropriate for this material if the preceding hypotheses are valid. At present no experimental data is available to validate this proposition.

No Region B damage has been identified for Inconel 718 in either Figs. 4, 5, or 7. It could be argued that the 0.1 mm demarcation for a crack is the cause of this discrepancy. For tensile loading cracks in a shear orientation range in size from 0.1 to 0.2 mm while on a scale of 1 mm crack growth is perpendicular to the maximum principal strain. Metallographic examination of the microstructure revealed grain size, dimensions ranging from 0.01 mm to 0.2 mm. Hence the initial dimension may correspond to either ten grains or a crack within a grain. Now if the crack is ten grains in dimension, most researchers will agree that it is a crack, while within a grain no consensus exists. The nagging question of when is a crack a crack persists.

It is not necessary for a material to display all three damage regions. Further implications are that if a Region A is experimentally determined at

shorter fatigue lives where shear cracking is a dominant life fraction, it does not infer that a shear based parameter such as Eq. (4) is appropriate when crack formation (i.e. Region C) is the dominant life fraction. Also, if Regions A and C are experimentally identified the existence of Region B for that material is not implied. Since most of the experimental data displays Region A damage accumulation, it is not surprising that adequate fatigue life estimates are obtained by implementing either Eq. (1) or (2). Minimal out-of-phase hardening is observed for low cycle fatigue of Inconel 718, hence comparable results are obtained for combinations of axial and torsional loads utilizing either Eq. (1) or (2). The high cycle fatigue ($>10^6$ cycles) behavior of this material is not well documented, but a trend indicating a change in damage mechanism for this life regime has been hypothesized.

Initial low cycle torsional fatigue testing ($<5 \times 10^4$ cycles) of AISI 304 stainless steel indicates shear crack growth dominated the damage accumulation process. At longer fatigue lives (5×10^4 to 10^7 cycles) Forsyth's Stage I cracks formed, but branched to a Stage II orientation for a dominant life fraction, indicating Region B fatigue damage. Although conceptually incorrect, considering the change in fatigue damage over the experimental life range for torsional loading, the data may be fit to either Eqs. (1), (2) or (3) with satisfactory results for a single state of stress. The changes in damage mode will be embedded in the material constants for each equation. Without considering the physical damage process it is difficult to correlate the data for different states of stress. An order of magnitude difference in fatigue life exists between torsional and axial experimental data in Fig. 10 for the same value of the shear damage parameter. Consideration of out-of-phase loadings increases the scatter of the data for this material when evaluating fatigue life with a shear parameter. Ignoring the dominant

physical fatigue damage process makes it difficult to correlate data for different states of stress.

Scanning electron microscopic examination of axial specimens [15] revealed brittle striations at the origin of fatigue damage for all fatigue lives greater than 10^3 cycles. Again the crack size used as a demarcation between crack initiation and propagation phenomena could be employed as an argument to suggest that a Region B exists for axial testing at shorter fatigue lives. Compared to a similar Stage II crack for torsional loading, crack propagation from a common dimension occupies a smaller life fraction for similar fatigue lives. However the brittle striations observed for initial crack formation in AISI 304 stainless steel for axial loadings could be construed such that it is interpreted that the damage accumulation during crack nucleation is dependent on principal stresses or strains. Even though it occupies a small life fraction, evidence of tensile type damage at the crack nucleation site could be hypothesized to be indicative of the damage occurring during crack nucleation. Alternately one could postulate that smaller dimensions of shear damage occur for tensile loading (much smaller than can be inferred by presently existing SEM fractography) and the same mechanism that caused a change in crack direction in torsion, occurs at a different dimension for axial loading. For either hypothesis implementation of the tensile model, Eq. (3), is appropriate. Both tension and torsional data can be correlated with this approach (Fig. 11).

Inconel 718 displayed similar damage accumulation for both tension and torsion over the fatigue life range experimentally investigated, but not AISI 304 stainless steel. However for the stainless steel, most of the experimental data falls within the Region B and Region C on the damage maps. Figure 11 shows an improved correlation of the fatigue data for AISI 304 stainless

steel employing Eq. (3). The modified Smith-Watson-Topper parameter previously showed promise as a damage analysis technique for materials such as cast iron where Stage II cracking dominates the damage accumulation. This would explain the success of this parameter when modeling the Region B damage observed for torsional testing and the Region C damage for axial loading.

Studies of the dislocation substructure for proportional and non-proportional loadings of AISI 304 stainless steel [28] indicate that this material is a planar slip material. The out-of-phase hardening which this material experiences has been explained via these dislocation observations. This suggests that cross slip is more difficult for this material, and may be partially responsible for the principal stress or strain dominated damage inferred from the choice of damage model (i.e. Eq. (3)). Where nominal plastic deformation occurs and nucleation phenomena dominate, implementation of Eq. (3) has been suggested for materials whose damage accumulation is best characterized by principal stresses. During the investigation of Inconel 718 combined axial-torsional loading, damage was shown to be bounded by axial and torsional loadings. Therefore after establishing the baseline damage characteristics of AISI 304 stainless steel via axial and torsional tests, the analytical and experimental focus of the research was on out-of-phase loadings. Again most of the experimental data corresponds to damage where Eq. (3) is suggested, and is reflected by the analytical success demonstrated in Fig. 11, for both in-phase and out-of-phase loadings.

Other researchers [29] have observed a change in dislocation structure from planar slip to cell structures at elevated temperatures (650 - 800°C). A change in fatigue damage could also be hypothesized at this increased temperature. This could imply that Eqs. (1), (2) or (4) (i.e. region A) would successfully model the damage phenomena (i.e. shear controlled) at the

elevated temperatures. When evaluating components that are thermally cycled, the temperature dependence of damage type could further complicate the analytical evaluation of actual service conditions with regard to fatigue life estimation.

Inconel 718 and AISI 304 stainless steel illuminate differences in damage accumulation commonly associated with classical brittle and ductile engineering metals. However, there are materials such as SAE 1045 steel that are considered to be ductile and display shear dominated fatigue damage accumulation [4,13]. Brittle materials such as cast iron [12] follow the classical concepts. Especially with non-ferrous alloys, it is important to investigate the individual material's fatigue damage accumulation rather than using rules of thumb developed for ferrous materials, the primary structural material prior to 1950. Over most of the fatigue life range both the Inconel 718 and stainless steel demonstrate damage accumulation that lends itself to correlation with a single damage parameter. Over another range of fatigue life neither of these materials may allow this convenience. However, this should not restrict the consideration of multiple damage regions. A complication that arises is how these regions of damage interact when variable amplitude fatigue cycling is analyzed. An understanding of these interactions will clarify many of the uncertainties associated with current cumulative damage methods. Surface cracking observations may suffice for low cycle fatigue interactions, but microscopic dislocation and microstructural evidence will probably provide more information for high-cycle fatigue interactions where testing time is prohibitive.

Previous observations have been for un-notched laboratory specimens. Most significant engineering applications involve a notch, or strain concentration. Some implications of the damage map concept will be summarized

in the following discussion. The traditional strain-life method considers uniaxial constant amplitude strain-life data as a baseline. Using Neubers hypothesis to account for non-linear notch deformation, a principal strain range is calculated. That is related to the uniaxial data in order to calculate a fatigue life. This is only conceptually in agreement with the damage map concept for Region B, and some Region C fatigue damage states. Often no consideration of notch constraint (e.g. plane stress or plane strain) is considered in the traditional strain-life approach. For some loading cases this factor may dictate the type of fatigue damage that occurs. Therefore even when considering notched members, damage maps afford the opportunity to choose the appropriate bulk stress/strain parameter based on the material, microstructure, and state of stress/strain for the loading amplitude.

For simple loading histories such as 90° out-of-phase tension torsion loading, the damage parameter can be interpreted in two ways. The damage parameter could always be evaluated on the plane experiencing the largest cyclic strain range. An alternate interpretation would compute the fatigue life for the largest value of the damage parameter including both cyclic strain and normal stresses. For in-phase loadings both interpretation result in identical results. For a variable amplitude history with a phase difference between some of the events, the shear or principal strain orientation experiencing the maximum damage may not correspond to the event with the maximum amplitude. A simple hypothetical example of this would involve one axial cycle, followed by only torsional fatigue cycles with a smaller shear strain amplitude (note: this also implies a smaller principal strain amplitude) than the axial loading. In a cumulative damage analysis for a shear dominated material the maximum shear strain orientation of the torsional cycles would experience a greater damage because of the larger

number of cycles than the maximum shear strain amplitude direction for the history, which corresponds to that for the axial loading. An orientation that does not correspond with the maximum principal stress or strain amplitude direction for the largest event in the history could be identified as the most damaging. For these situations, the value of the entire bulk stress-strain parameter could be evaluated for all possible orientations, with the direction of the maximum damage for the history being interpreted as the anticipated direction of fatigue cracking. Damaging events would be inferred from a closed path in nominal stress/strain space. Again it is conceivable that an orientation that does not correspond to the maximum appropriate stress or strain amplitude direction for any individual event in the history could be identified as the most damaging. Also, for this method it is possible to predict an orientation that does not correspond to the maximum amplitude of the primary damage parameter for a loading that involves repetitions of a single event [15].

The dimension of some components may result in tensile or shear long crack propagation being a dominant fatigue life fraction, even if it is not so identified from damage maps constructed from unnotched laboratory specimens. For these cases a mixed mode fracture mechanics approach is probably adequate to insure that life predictions are not overly conservative. In order to improve fatigue life estimation techniques for simple and more complex stress states, a knowledge of the type of fatigue damage that occurs for a given material and loading is essential.

CONCLUSIONS

The concept of fatigue damage maps, analogous to fracture maps of Ashby et al. [30] has been employed to characterize fatigue damage. Material, state of stress and/or strain, loading amplitude, and microstructure all influence the type of fatigue damage observed. Hydrostatic stress has been used to summarize three major categories (shear crack growth, tensile crack growth, and crack nucleation) of fatigue damage from various stress-strain states. Successful extrapolation of data from simple to more complex constant amplitude loadings has required that similar fatigue damage occurs for both stress-strain states. When this similarity in damage exists for a material, appropriate bulk stress-strain parameters are used to correlate both in-phase and out-of-phase experimental data. Further research is required to extend these concepts to general variable amplitude loadings.

REFERENCES

1. Guard, Y. S., "Multiaxial Fatigue: A Survey of the State of the Art," Journal of Testing and Evaluation. Vol. 9, No. 3, 1981, pp. 165-178.

2. Krempl, E., "The Influence of State of Stress on Low-Cycle Fatigue of Structural Materials: A Literature Survey and Interpretive Report." ASTM STP 549, American Society for Testing and Materials, Philadelphia, 1974, 46 pp.

3. Wöhler, A., Zeitschrift für Bauwesan, Vol. 8, 1858, p. 641.

4. Ewing, J. A., and J. C. W. Humphrey, "The Fracture of Metals and Repeated Alterations of Stress," Philosophical Trans. of the Royal Society of London, Series A, Vol. 200, 1903, Part 1, pp. 241-250.

5. Forsyth, P. J. E., "A Two Stage Process of Fatigue Crack Growth," Proceedings of the Symposium on Crack Propagation, Cranfield, England, 1961, pp. 76-94.

6. Gough, H. J., "Crystalline Structure in Relation to the Failure of Metals-Especially Fatigue," Proc. ASTM, Vol. 33, Part II, 19XX, pp. 3-14.

7. Guest, J. J., "Recent Research on Combined Stress," Proceedings Institution of Automobile Engineers, Vol. 35, Dec. 1940, pp. 33-72 and 146-171.

8. Jacquelin, B., Hourlier, F., and Pineau, A., "Crack Initiation under Low-Cycle Multiaxial Fatigue in Type 316L Stainless Steel," Transactions ASME, Vol. 105, 1983, pp. 138-143.

9. Forsyth, P. J. E., "Fatigue Damage and Crack Growth in Aluminum Alloys," ACTA Metallurgica, Vol. 11, 1963, pp. 703-715.

10. Fash, J. W., "Fatigue Crack Initiation and Growth in Gray Cast Iron," Fracture Control Program, Report No. 35, College of Engineering, University of Illinois at Urbana-Champaign, 1980, pp. 47-50.

11. Dowling, N. E., "Crack Growth during Low-Cycle Fatigue of Smooth Axial Specimens," Cyclic Stress-Strain and Plastic Deformation Aspects of Fatigue Crack Growth, ASTM STP 637, American Society for Testing and Materials, 1977 pp. 97-112.

12. Bannantine, J. A., and Socie, D. F., "Observations of Cracking Behavior in Tension and Torsion Low Cycle Fatigue," presented at ASTM Symposium on Low Cycle Fatigue-Directions for the Future, to be published as an STP, American Society for Testing and Materials, Philadelphia, 1985.

13. Hua, C. T., and Socie, D. F., "Fatigue Damage in 1045 Steel Under Constant Amplitude Biaxial Loading," Fatigue of Engineering Materials and Structures, Vol. 2, No. 3, 1984, pp. 165-179.

14. Socie, D. F., Kurath, P., and Koch, J., "A Multiaxial Fatigue Damage Parameter," presented at the Second International Symposium on Multiaxial Fatigue, Sheffield, U.K., 1985.

15. Jones, D. J., and Kurath, P., "Cyclic Fatigue Damage Characteristics Observed for Simple Loadings Extended to Multiaxial Life Predictions," NASA Publication NASA/CR/182126, 1988.

16. Nadia, A., Plasticity, A Mechanics of the Plastic State of Matter, McGraw-Hill Book Co., Inc., New York, 1931.

17. Findley, W. N., Mather, P. N., and Martin D. E., "Fatigue Failure under Combinations of Stresses," Theoretical and Applied Mechanics Report No. 61, University of Illinois, 1954.

18. Orowan, E., Dislocations in Metals, The American Institute of Mining and Metallurgical Engineers, Inc., New York, NY, 1954, pp. 188-194.

19. Kandil, F. A., Brown, M. W., and Miller, K. J., "Biaxial Low-Cycle Fatigue of 316 Stainless Steel at Elevated Temperatures," The Metals Society, Vol. 280, London, 1982, pp. 203-210.

20. Socie, D. F., and Shield, T. W., "Mean Stress Effects in Biaxial Fatigue of Inconel 718," ASME Journal of Engineering Materials and Technology, Vol. 106, 1984, pp. 227-232.

21. Fatemi, A., and Socie, D. F., "A Critical Plane Approach to Multiaxial Fatigue Damage Including Out-of-Phase Loading," to be published in the Journal of Fatigue and Fracture of Engineering Materials and Structures, 1987.

22. Fatemi, A., and Kurath, P., "Multiaxial Fatigue Life Predictions under the Influence of Mean Stresses," submitted to the ASME Journal of Engineering Materials and Technology, 1987.

23. Smith, K. N., Watson, P., and Topper, T. M., "A Stress-Strain Function for the Fatigue of Metals," Journal of Materials, Vol. 5, No. 4, 1970, pp. 767-778.

24. Nisitani, H., Japan Society of Mechanical Engineers Bulletin, Vol. 11, No. 48, 1968, pp. 947-957.

25. Nisitani, H., and Kawano, K., Japan Society of Mechanical Engineers Bulletin, Vol. 15, No. 82, 1972, pp. 433-438.

26. Morrow, D. L., "Biaxial-Tension Fatigue of Inconel 718," Ph.D. Thesis, Department of Mechanical Engineering, University of Illinois at Urbana-Champaign, 1987, 113 pp.

27. Bashir, Shahid, "High Temperature Low Cycle Fatigue of Nickel Based Superalloys Rene '95 and Inconel 718," Ph.D. Thesis, Department of Materials Science and Metallurgical Engineering, University of Cincinnati, Cincinnati, OH 1982, 189 pp.

28. Doong, S. H., Socie, D. F., and Roberson, I. M., "Dislocation Substructures and Nonproportional Hardening," submitted to ASME Journal of Engineering Materials and Technology, 1988.

29. Challenger, K. D., and Moteff, J., "Correlation of Substructure with the Elevated Temperature Low Cycle Fatigue of AISI 304 and 316 Stainless Steels," Fatigue at Elevated Temperatures, ASTM STP 520, American Society for Testing and Materials, Philadelphia, PA, 1973, pp. 68-79.

30. Ashby, M. F., Embury, J. D., Coohsley, S. H., and Teirlink, D., "Fracture Usages with Pressure as a Variable," Scripta Metallurgical, Vol. 19, 1985, pp. 385-390.

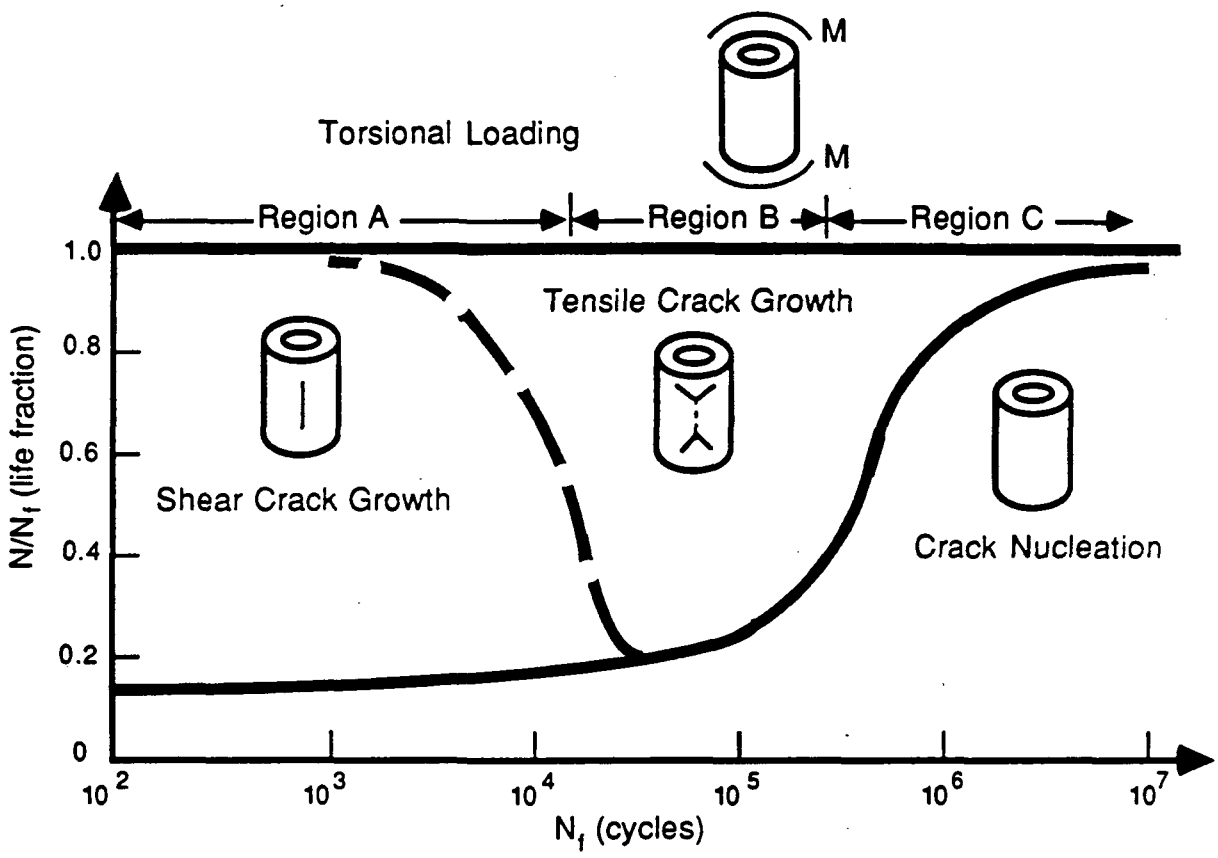

Fig. 1 Hypothetical fatigue damage map for torsional loading

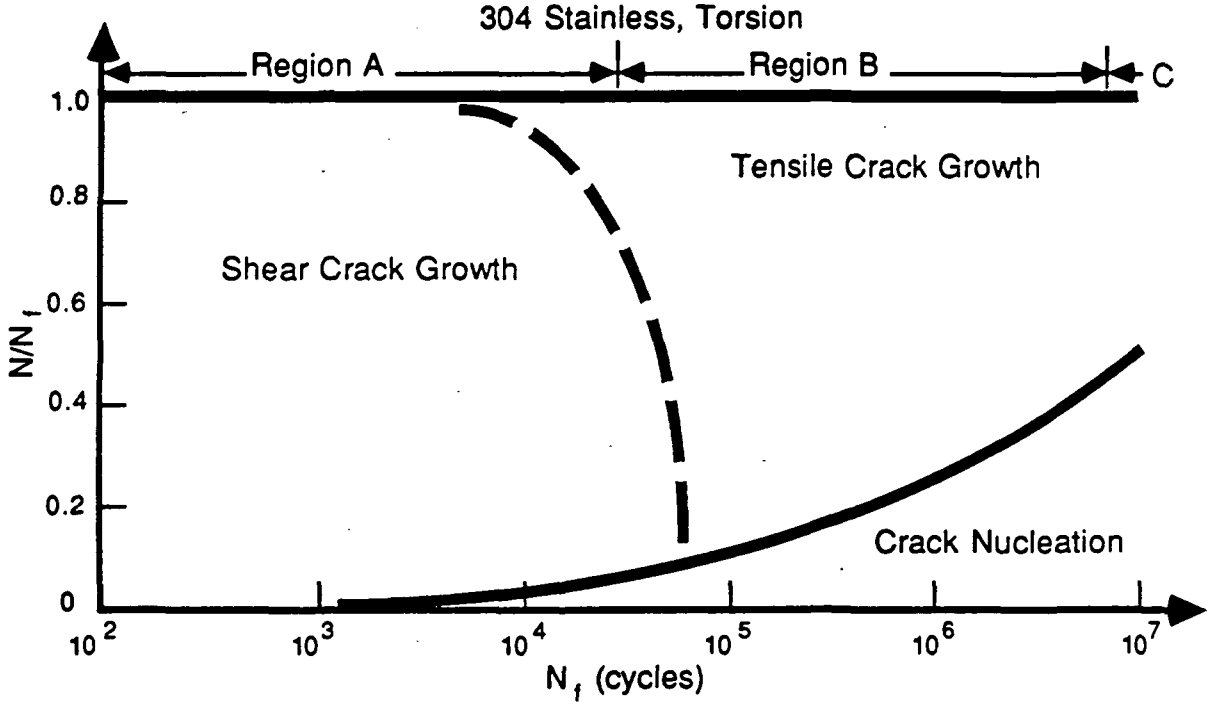

Fig. 2 Fatigue damage for torsional loading of AISI 304 stainless steel

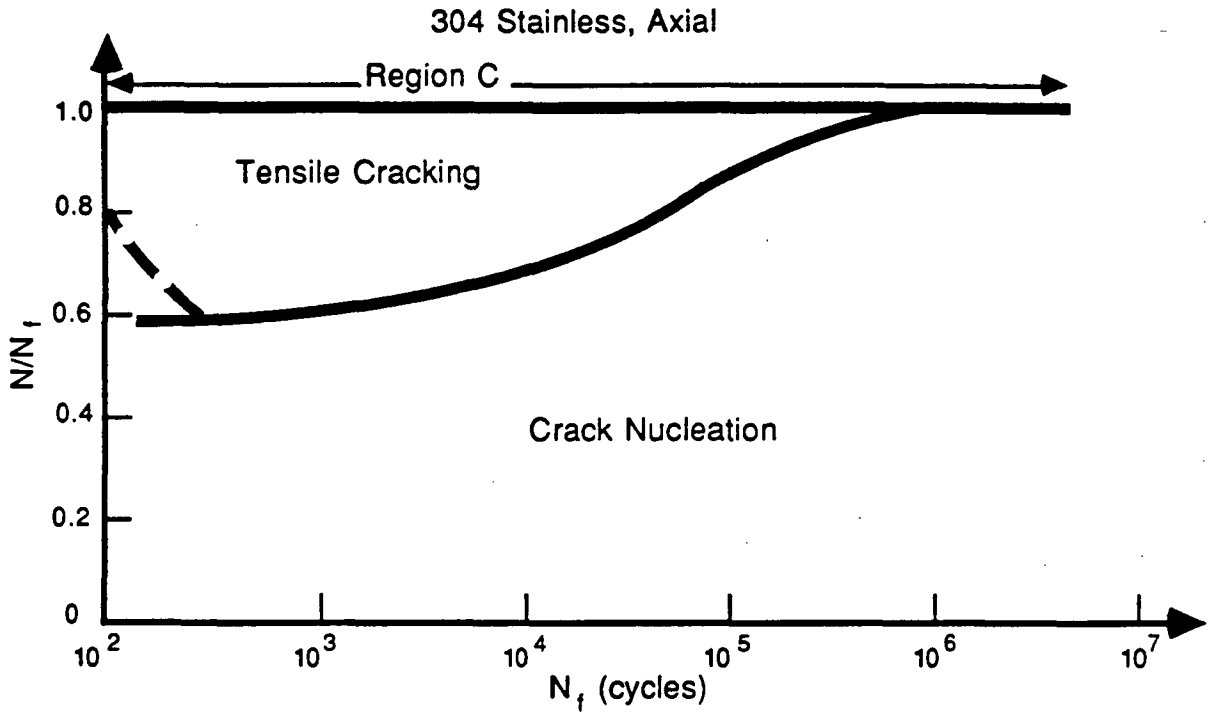

Fig. 3 Fatigue damage for axial loading of AISI 304 stainless steel

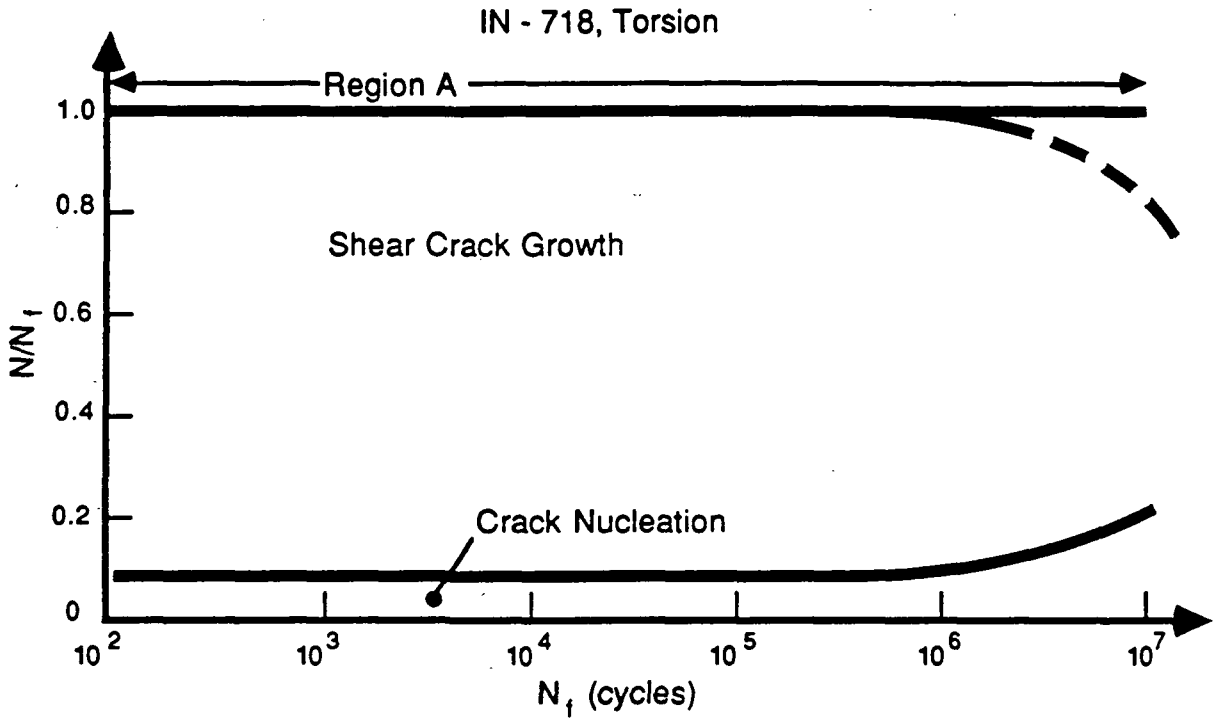

Fig. 4 Fatigue damage for torsional loading of Inconel 718

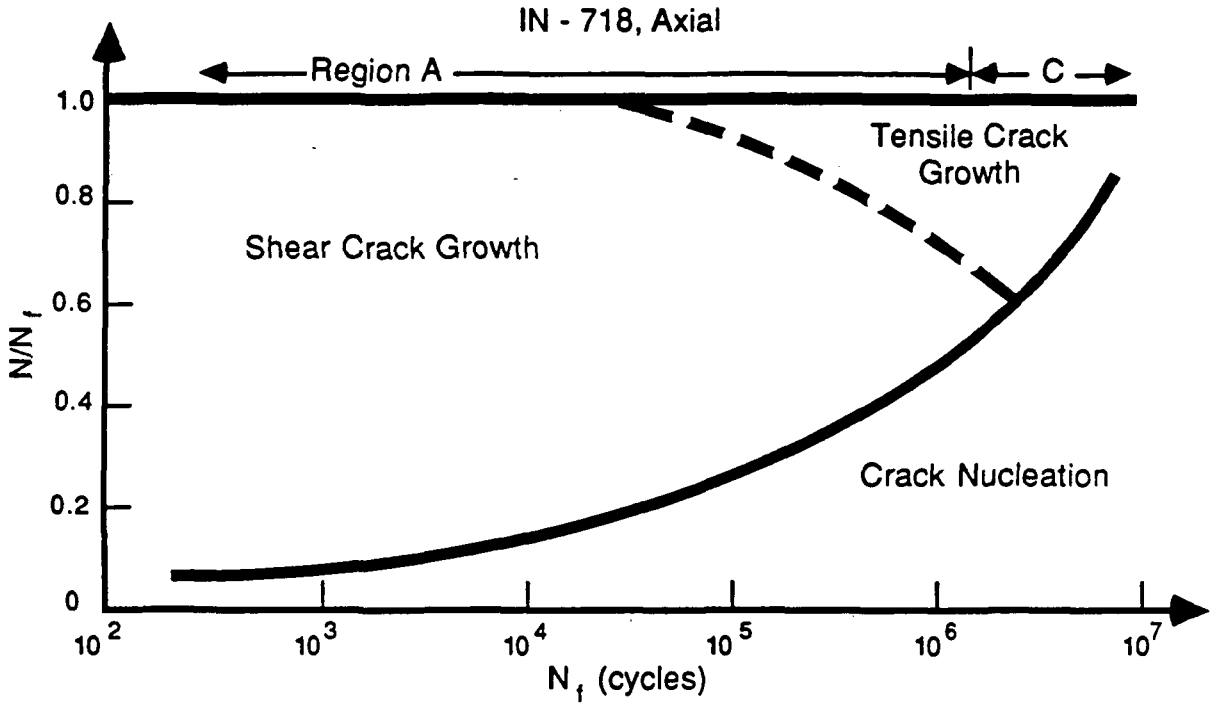

Fig. 5 Fatigue damage for axial loading of Inconel 718

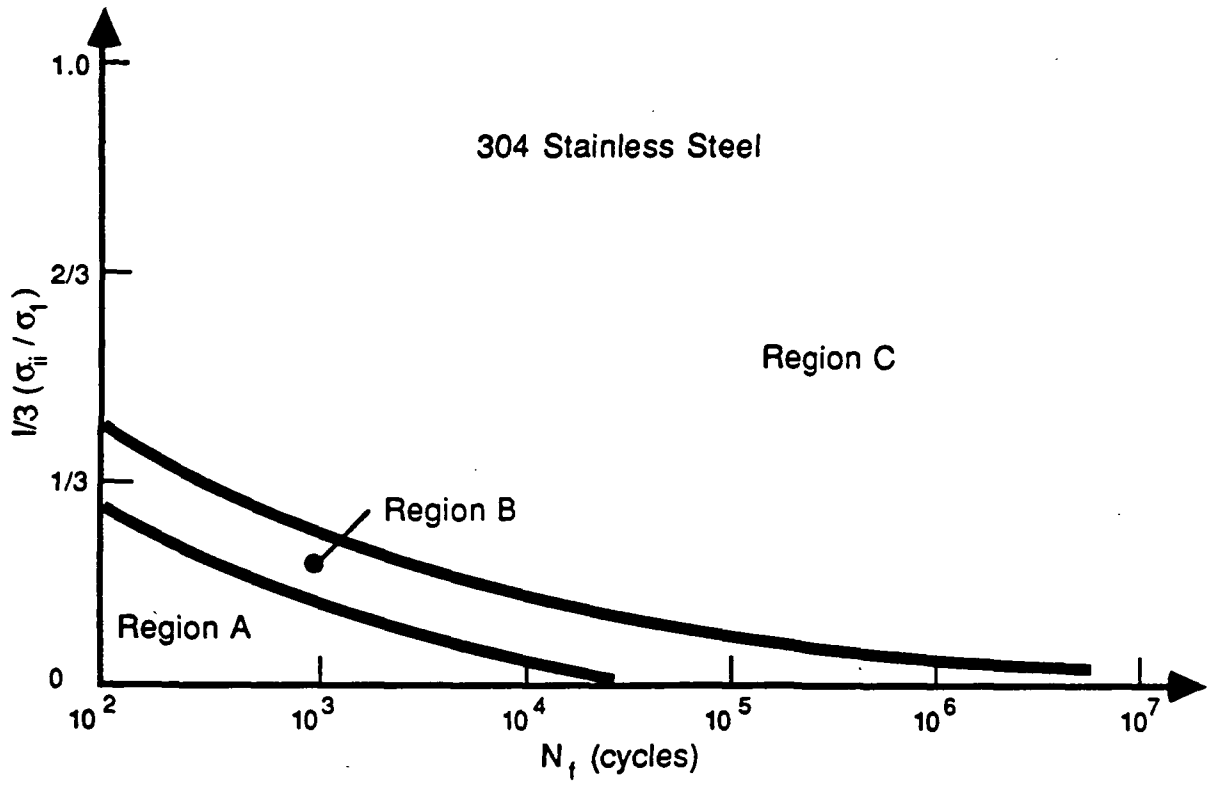

Fig. 6 Fatigue damage map for AISI 304 stainless steel

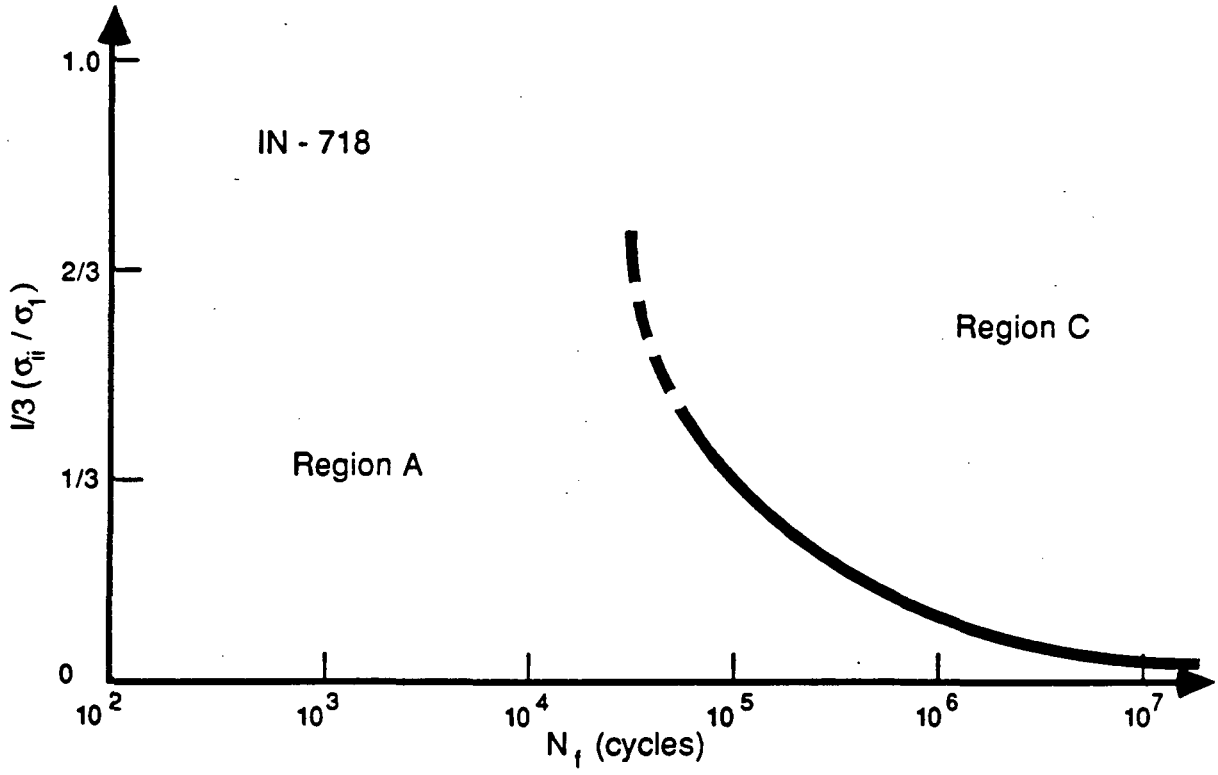

Fig. 7 fatigue damage map for Inconel 718

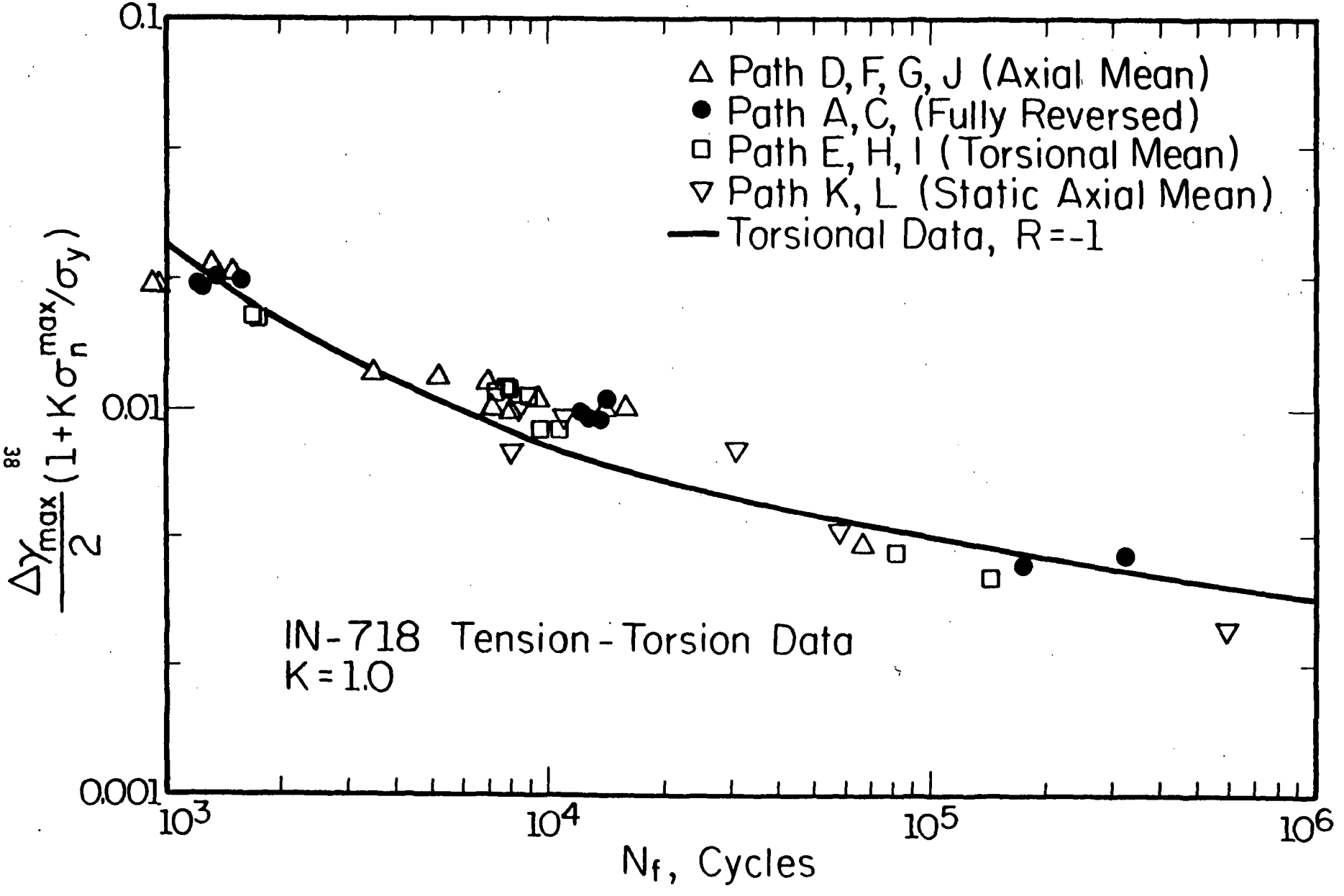

Fig. 8 Correlation of the Inconel 718 experimental data employing a shear fatigue damage parameter

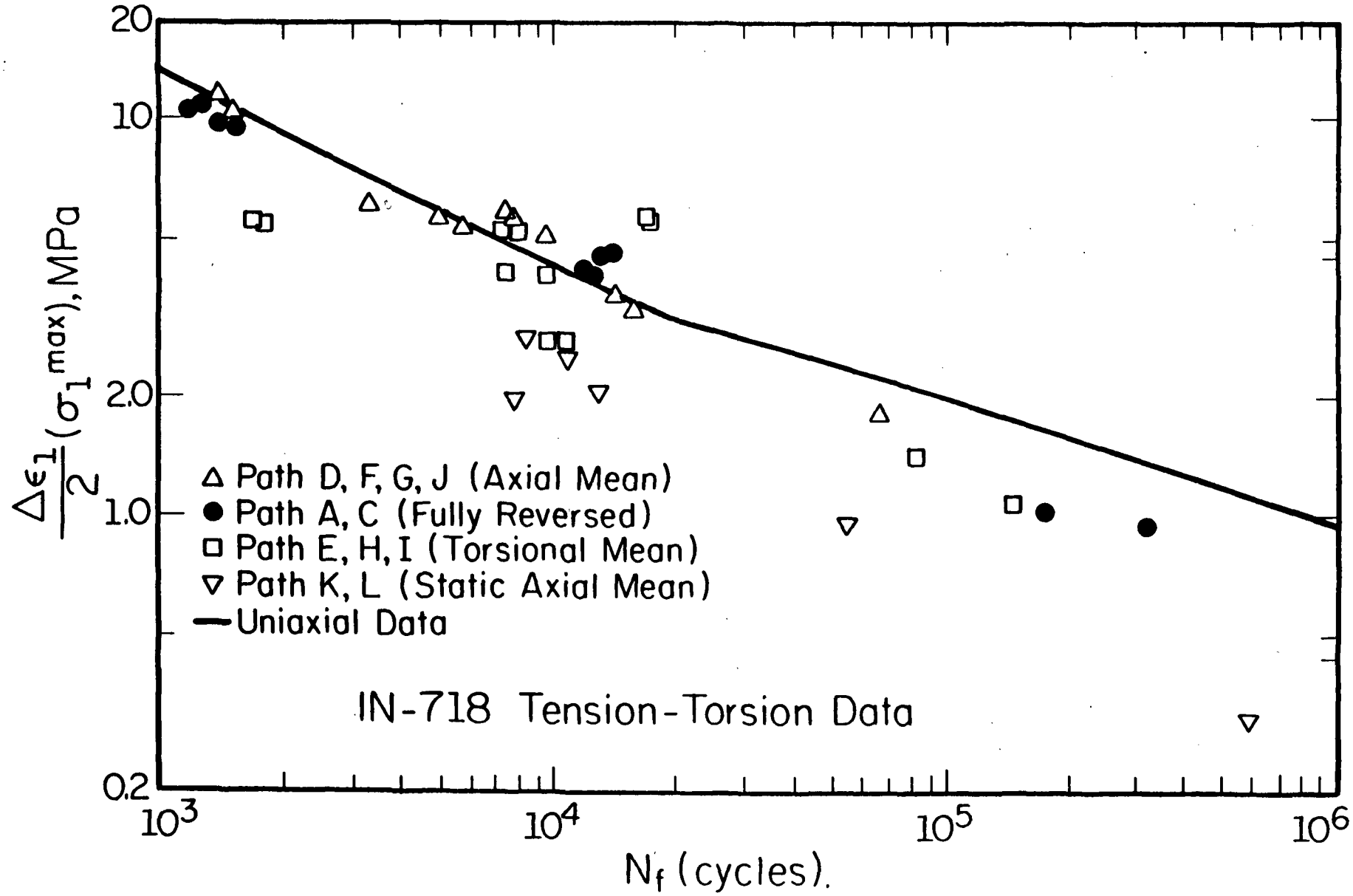

Fig. 9 Correlation of the Inconel 718 experimental data employing a principal strain fatigue damage parameter

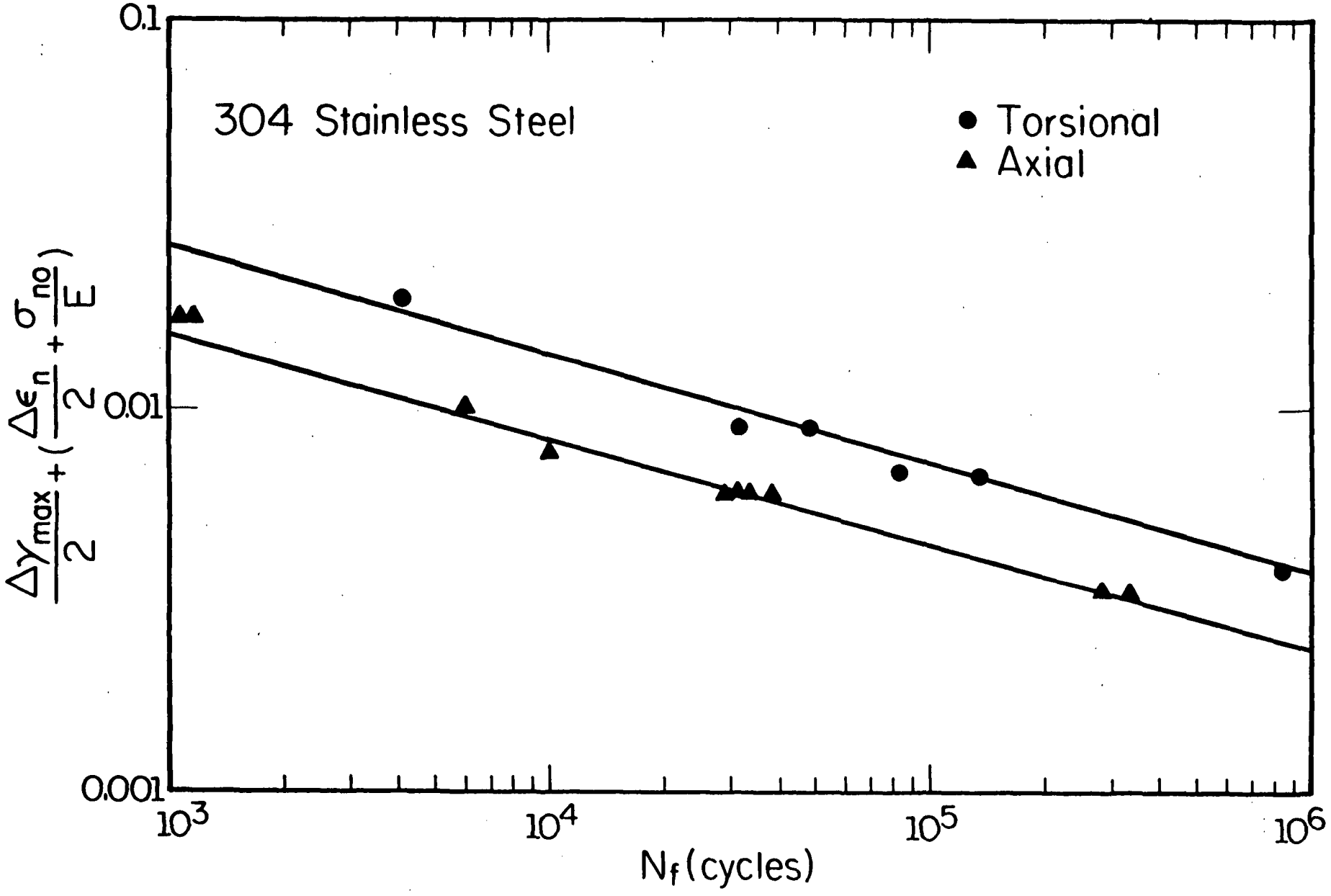

Fig. 10 Correlation of the AISI 304 stainless steel data using a shear fatigue damage parameter

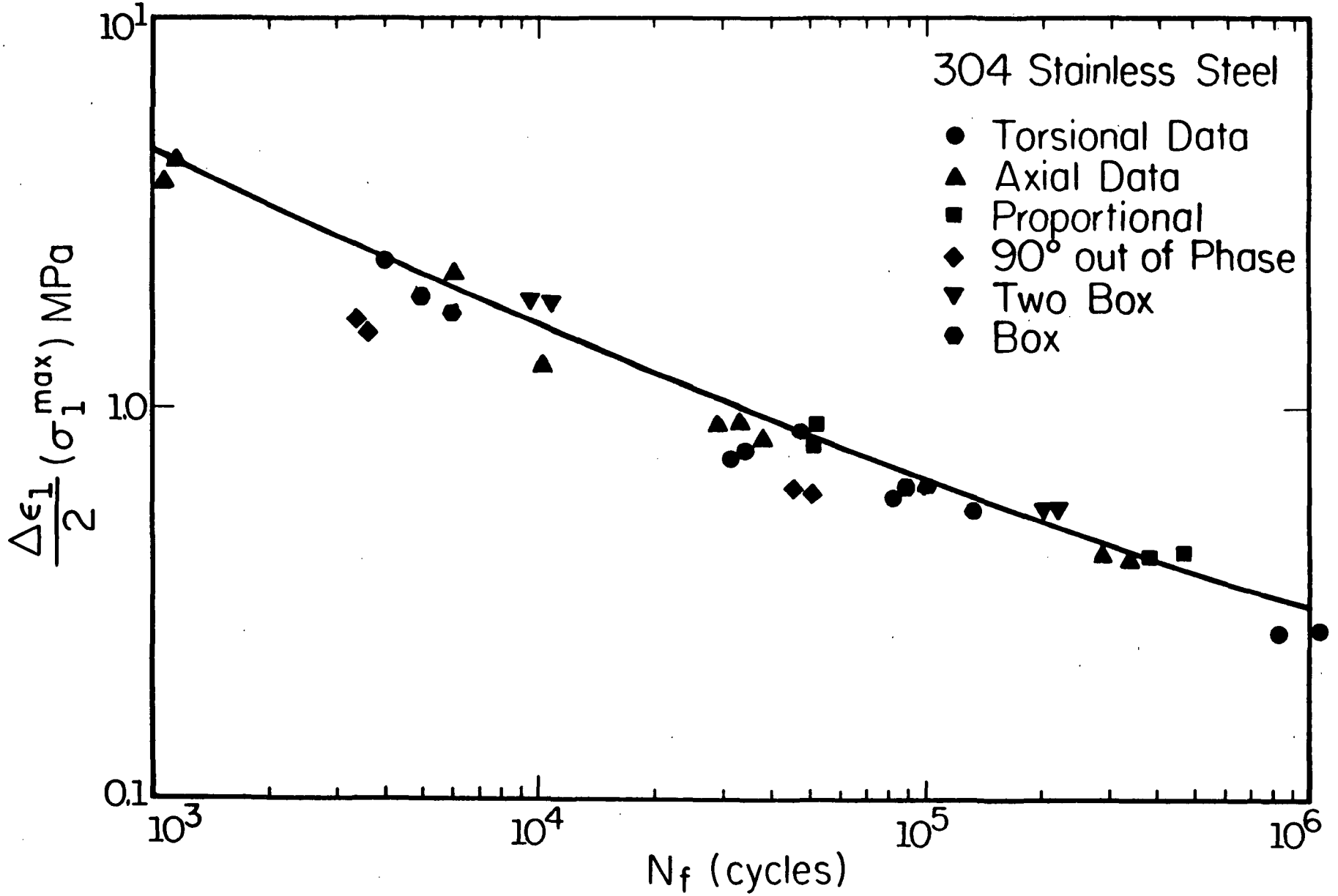

Fig. 11 Correlation of the AISI 304 stainless steel data using a principal strain fatigue damage parameter

NASA
National Aeronautics and Space Administration

Report Documentation Page

1. Report No.	2. Government Accession No.	3. Recipient's Catalog No.
NASA CR-182191		

4. Title and Subtitle
The Relationship Between Observed Fatigue Damage and Life Estimation Models

5. Report Date
August 1988

6. Performing Organization Code

7. Author(s)
Peter Kurath and Darrell F. Socie

8. Performing Organization Report No.
None

10. Work Unit No.
505-63-1B

9. Performing Organization Name and Address
University of Illinois at Urbana-Champaign
Department of Mechanical and Industrial Engineering
Urbana, Illinois 61801

11. Contract or Grant No.
NAG3-465

13. Type of Report and Period Covered
Contractor Report
Final

12. Sponsoring Agency Name and Address
National Aeronautics and Space Administration
Lewis Research Center
Cleveland, Ohio 44135-3191

14. Sponsoring Agency Code

15. Supplementary Notes
Project Manager, Alan D. Freed, Structures Division, NASA Lewis Research Center.

16. Abstract

Observations of the surface of laboratory specimens subjected to axial and torsional fatigue loadings has resulted in the identification of three fatigue damage phenomena; crack nucleation, shear crack growth, and tensile crack growth. Material, microstructure, state of stress/strain, and loading amplitude all influence which of the three types of fatigue damage occurs during a dominant fatigue life fraction. Fatigue damage maps are employed to summarize the experimental observations. Appropriate bulk stress/strain damage parameters are suggested to model fatigue damage for the dominant fatigue life fraction. Extension of the damage map concept to more complex loadings is presented.

17. Key Words (Suggested by Author(s))	18. Distribution Statement
Fatigue Multiaxial fatigue Damage maps	Unclassified – Unlimited Subject Category 39

19. Security Classif. (of this report)	20. Security Classif. (of this page)	21. No of pages	22. Price*
Unclassified	Unclassified	41	A03

*For sale by the National Technical Information Service, Springfield, Virginia 22161

NASA